Thermoplastic Elastomers from iPP/EPR Blends: Crystallization and Phase Structure Development

L. D'ORAZIO, C. MANCARELLA, E. MARTUSCELLI,* G. STICOTTI, and R. GHISELLINI†

Istituto di Ricerche su Tecnologia dei Polimeri del C.N.R., Via Toiano, 6 80072 Arco Felice, Napoli, Italy

SYNOPSIS

The phase morphology and structure of thermoplastic elastomers obtained from isotactic polypropylene (iPP) and ethylene–propylene random copolymer (EPR) blends by means of the dynamic curing of EPR rubbery component carried out during its melt mixing with iPP in a Banbury mixer at 180°C were investigated. Samples obtained by compression molding and by using isothermal crystallization conditions of the iPP phase were analyzed by means of differential scanning calorimetry, of optical, scanning, and transmission electron microscopy, and of wide-angle and small-angle X-ray diffraction. The influence of cooling below the melting point and of EPR molecular structure on the kinetic and thermodynamic parameters related to crystallization process of the iPP phase was also studied. It was found that the process of dynamic curing of the EPR component dramatically affects the development of the phase morphology and structure in the material. As a matter of fact, the blend containing the uncured EPR is characterized by the presence of iPP domains randomly distributed in the EPR rubbery matrix, whereas in the blend containing the cured EPR the iPP phase becomes the continuous phase crystallizing in a structure that resembles a cobweb tending to surround the EPR cured particles; moreover such an iPP cobweb appears to be constituted by row structures of stacked lamellae. It was found that the addition of EPR phase interferes dramatically with the crystallization process of the iPP, thus inducing drastic modification in its intrinsic morphology (size, neatness, regularity of spherulites, inner structure of spherulites, etc.). Such interference was found to be comparatively stronger when the iPP phase crystallizes in presence of cured EPR. The elastic behavior of the thermoplastic elastomer material was accounted for by applying the "leaf spring model" to the morphology and structure of the iPP phase crystallized in presence of cured EPR.

INTRODUCTION

Thermoplastic elastomers[1,2] are rubbery materials that are processable as simple thermoplastic materials but exhibit properties similar to those of a vulcanized elastomer at use temperature. During recent years such materials, offering the advantage of being turned directly into finished goods, have attracted growing interest.

An effective way to produce thermoplastic elastomeric compositions consists in creating a multicomponent system with vulcanized elastomer particles included in a melt-processable plastic matrix by means of the method called "dynamic vulcanization." In this process the vulcanization of the rubbery component occurs during its mixing with a nonvulcanizable thermoplastic polymer. The dynamic vulcanization process was at first used by Gessler[3] in the preparation of "semirigid" elastomer-plastic compositions containing varying amounts of partially vulcanized elastomer. Fisher's work[4-6] has led to thermoplastic elastomers from a crosslinked blend of ethylene-propylene-diene copolymer (EPDM) and crystalline polypropylene. Hartman developed thermoplastic elastomers based on butyl rubber and polyethylene.[7,8] More recently thermoplastic highly elastomeric compositions of EPDM and polypropylene have been prepared by dynamic vulcanization.[9,10]

* To whom correspondence should be addressed.
† Present address: Himont, Ferrara, Italy.

Journal of Applied Polymer Science, Vol. 53, 387–404 (1994)
 CCC 0021-8995/94/040387-18

In 1990 Braga et al. developed a dynamic vulcanization process to obtain thermoplastic elastomers from isotactic polypropylene (iPP) and ethylene–propylene random copolymer (EPR) blends.[11]

In the present work results of a study dealing with thermoplastic elastomers prepared from iPP–EPR blends by means of the dynamic vulcanization process described in Ref. 11 are reported.

The work was undertaken to assess the phase morphology and structure of the blends, before and after dynamic curing of EPR component developed in samples obtained by compression molding and in samples with the iPP phase able to crystallize isothermally.

The effects of cooling below the melting point and EPR molecular structure on the kinetic and thermodynamic parameters related to the isothermal crystallization process of the iPP phase were also examined.

EXPERIMENTAL

Materials

The starting polymers used in this study were an isotactic polypropylene (iPP) (X30G) made by Himont, having a melt flow index equal to 8 g/10 min and an ethylene–propylene random copolymer (EPR), supplied by Himont, with a Mooney viscosity ML (1 + 4) at 121°C equal to 130 and a propylene content (C_3) of 44% wt/wt.

Blending and Sample Preparation

Binary blends with a composition of EPR–iPP 70/30 (wt/wt) (code A) and blends to which a peroxide rubber curing agent was added, with a composition EPR–iPP–peroxide 67/29/4 (wt/wt) (code B) were prepared. Sample A was obtained by mixing the iPP and the EPR copolymer in a Banbury mixer at 180°C with a blending time of 10 min. Sample B was obtained by adding the curing agent to iPP and EPR mixed for 10 min in the mixer at 180°C and mixing for a further 10 min. After blending, the materials were compression molded at 220°C into sheets $\approx$ 2 mm thick.

Techniques

Differential Scanning Calorimetry

The thermal behavior of materials studied was analyzed by means of a differential scanning calorimeter (DSC) Mettler TA 3000 equipped with a control and programming unit (microprocessor Tc 10). The glass transition temperature (T_g), the apparent melting temperature (T'_m), and the crystallinity index of compression-molded samples of the neat iPP and iPP–EPR blends were determined following this procedure: the samples (about 9–10 mg) were heated from −100°C up to 215°C with a rate of 10°C/min, and the heat (dH/dt) evolved during the scanning process was recorded as a function of temperature. The T_g was taken as the temperature corresponding to 50% of the transition. The observed melting temperature (T'_m) and the apparent enthalpies of melting ΔH^* were obtained from the maxima and the area of the melting peaks, respectively. The crystallinity index (X_c) of iPP phase and of blends were calculated by applying the following relations:

$$X_c(\text{iPP}) = \frac{\Delta H^*(\text{iPP})}{\Delta H^\circ(\text{iPP})}$$

$$X_c(\text{blend}) = \frac{\Delta H^*(\text{blend})}{\Delta H^\circ(\text{iPP})}$$

where ΔH^*(iPP) is the apparent enthalpy of fusion per gram of iPP in the blend; ΔH°(iPP) is the heat of fusion per gram of 100% crystalline iPP from[12] ΔH°(iPP) = 209 J/g, and ΔH^*(blend) is the apparent enthalpy of fusion per gram of blend. The effect of nucleating ability of EPR and cured EPR copolymers on crystallization process of iPP was investigated following this procedure: the samples were heated up to 215°C with a rate of 20°C/min and kept at this temperature for 15 min and then cooled with a rate of 10°C/min.

The apparent melting temperature (T'_m) and the crystallinity index of the neat iPP [X_c(iPP)] and iPP crystallized isothermally at 124, 134, and 139°C from its blends in the presence of EPR and cured EPR copolymers [X_c(blend)] were determined following this procedure: the samples were heated to 215°C at a rate of 20°C/min and kept at this temperature for 15 min in order to destroy any trace of crystallinity; then they were rapidly cooled to the desired crystallization temperature; after complete crystallization such samples were again heated to 215°C at a rate of 10°C/min. The observed melting temperature (T'_m) and the crystallinity index of iPP phase and of blends were determined as described above.

Optical Microscopy

The overall morphology, developed in samples of pure iPP and iPP–EPR blends isothermally crystallized from melt at temperatures of 124, 134, and 139°C and of nonisothermally crystallized samples,

was analyzed by means of optical microscopy. A Leitz optical polarizing microscope fitted with a Mettler hot stage was used. The following procedure was employed: thin films, obtained by squeezing the materials between a microscope slide and a cover glass, were heated up to 200°C and kept at this temperature for 10 min to destroy any trace of crystallinity; the temperature was then rapidly lowered to the desired T_c and the material allowed to crystallize isothermally. Nonisothermally crystallized samples were obtained by quenching the melts in air. Optical micrographs were taken with crossed and parallel polarizers.

Scanning Electron Microscopy

Cryogenically fractured surfaces of parallelepipedal-shaped specimens about 1 mm thick, nonisothermally crystallized, were observed by means of a Philips 501 scanning electron microscope (SEM) after coating with Au–Pd in a sputtering Polaron equipment LTD E S/50. To elucidate more deeply, the phase structure developed in the blend sample obtained after the dynamic curing reaction of the EPR component, a selective dissolution of the uncured EPR phase, by means of boiling xylene vapors, was also carried out on cryogenically fractured surfaces of sample B. It was, in fact, found that the iPP phase remains unaffected by xylene vapors for long exposure time (30 min). The etched surfaces were, subsequently, SEM analyzed.

Transmission Electron Microscopy

Ultrathin sections (about 150 Å thick) of nonisothermally crystallized sample B, cut by means of a LKB Ultratome V ultramicrotome equipped with a diamond knife operating at −130°C, were observed by means of a Philips 301 transmission electron microscope (TEM) after staining with RuO_4.

Wide-Angle X-Ray Scattering

Wide-angle X-ray scattering (WAXS) studies, performed on samples of the neat iPP and iPP isothermally crystallized from its blends with EPR copolymer and with cured EPR copolymer at 124, 134, and 139°C, were carried out by means of a PW 1060/71 Philips diffractometer (CuKα Ni-filtered radiation); the high voltage was 45 KV and the tube current was 25 mA.

Small-Angle X-Ray Scattering

Small-angle X-ray scattering (SAXS) studies performed on samples of the neat iPP and iPP isothermally crystallized from its blends with EPR copolymer and with cured EPR copolymer at 124, 134, and 139°C were carried out by means of a compact Kratky camera equipped with a Braun one-dimensional positional sensitive detector. Ni-filtered CuKα radiation generated from a Philips X-ray generator (PW 1730/10) operating at 40 KV and 30 μA, was used. The raw scattering data were corrected for parasitic scattering, absorption, and slit smearing by using Vonk's method.[13] The desmeared intensities were then Lorentz factor corrected by multiplying by s^2 ($s = 2 \sin \theta/\lambda$).[14]

Uniaxial Tensile Testing

Stress–strain curves of the plain iPP and B samples were obtained at room temperature by means of an Instron 4502 according to ASTM D 638; rates of 50 and 500 m/min were used for the iPP and B samples, respectively.

RESULTS AND DISCUSSION

Thermal Behavior

The DSC thermograms of compression-molded samples of the neat iPP and iPP–EPR blends show a single T_g and a single endothermic peak when heated from −100 to 215°C. Such T_g's and the temperature position of the peaks observed (T'_m) are reported in Table I together with the T_g of the starting plain blend components and the crystallinity index of the iPP–EPR blends [X_c(blend)] and of the iPP phase [X_c(iPP)]. As shown in Table I, the T_g values are located at −54°C (sample A) and −55°C (sample B) and are to be attributed to the EPR phase. Note that the T_g shown by the EPR component in the blends is quite comparable to that shown by the plain EPR with no dependence on the EPR molecular structure.

The neat iPP, and iPP crystallized in the presence of EPR, exhibit almost the same values of T'_m. Such

Table I Glass Transition Temperature, T_g, Observed Melting Temperature, T'_m, Overall Blend Crystallinity, X_c Blend, and Index of Crystallinity (X_c (iPP) for Plain iPP, EPR Copolymer, and iPP–Uncured EPR Blend (A) and iPP–Cured EPR Blend (B)

Sample	T_g (°C)	T'_m (°C)	X_c (Blend)	X_c (iPP)
iPP	−10	164	—	36
EPR	−53	—	—	—
A	−54	163	10	33
B	−55	153	9	32

findings are in agreement with results obtained in previous work studying different (80/20) iPP–EPR blends,[15] the melting behavior of the iPP phase in iPP–EPR blends is independent of overall blend composition and EPR molecular mass: the perfection and the thickness of the growing iPP crystals is not influenced by the presence of the EPR phase. Thus, according to Martuscelli,[16,17] iPP and EPR copolymers are confirmed to be immiscible in the molten state.

A noticeable depression in T'_m value is, on the contrary, shown by the iPP phase crystallized in the presence of cured EPR (see Table I) indicating that more defective and/or thinner lamellar crystals are formed. Such a finding could be ascribed to the presence of the cured EPR phase that influences the crystallization process of the iPP phase and/or to the probable branching undergone by means of the curing agent by the iPP phase during the dynamic curing process. Work is in progress to clarify whether the observed differences between the polypropylene of A blend and the polypropylene of B blend are due to the crosslinking of the EPR phase or due to the degradation of the iPP.

As shown in Table I, the X_c(blend) values closely approach each other and, as expected, are much lower than that shown by the plain iPP. Moreover, note also that the X_c(iPP) values remain lower than those shown by the plain iPP, a comparatively lower value being shown by the blend sample containing the cured EPR. Such results are in agreement with results obtained while studying different iPP–EPR blends:[15] the crystallization process of iPP from its blends with EPR is influenced by the presence of the rubbery phase. Such an influence seems to become stronger when the EPR phase is cured.

The nonisothermal crystallization curves of the plain iPP and iPP–EPR blends are shown in Figure 1. As shown, the plain iPP crystallizes between 133 and 102°C, the temperature position of the maximum of the peak being at $\approx$ 116°C. It is interesting to note that when the iPP crystallizes in the presence of EPR the crystallization peak shifts to lower temperature, ranging between 123 and 92°C [compare Fig. 1(a) with Fig. 1(b)] whereas the range of crystallization temperature shown by iPP crystallizing in the presence of cured EPR (132–104°C) remains quite comparable to that shown by the plain iPP [compare Fig. 1(a) with Fig. 1(c)]. Such findings indicate that the EPR used in this work has no nucleating ability on the crystallization process of the iPP; a migration of heterogeneous nuclei from the iPP phase toward the EPR phase occurring. By curing the EPR phase, such a migration is no longer observed.

The DSC thermograms of samples of the neat iPP and iPP–EPR blends isothermally crystallized at 124, 134, and 139°C show relatively broad endothermic peaks when heated from the crystallization temperature to 215°C; the temperature position

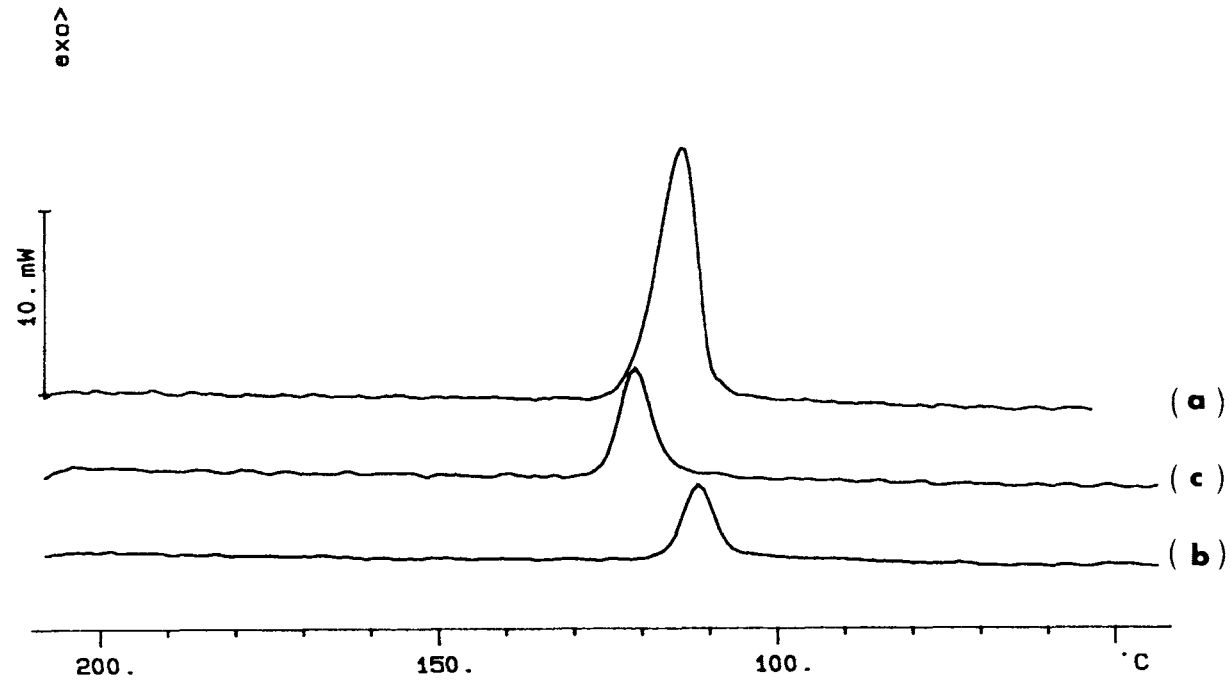

Figure 1 Nonisothermal crystallization curves of (a) plain iPP, (b) blend A, (c) blend B.

Table II Observed Melting Temperature, T'_m, for Plain iPP and iPP Crystallized Isothermally from Its Blends with EPR Copolymer (A) and Cured EPR Copolymer (B) as a Function of Crystallization Temperature, T_c

	T'_m (°C)		
Sample	T_c = 124°C	T_c = 134°C	T_c = 139°C
iPP	161	165	170
A	161	164	163
B	154	157	159

of maxima of these peaks (T'_m) are reported in Table II. As shown in Table II, the T'_m values of the neat iPP are characteristic of the melting of the α crystalline forms of iPP and, as expected, increase with increasing T_c. As far as the melting behavior of the two blends is concerned, they behave very differently. As a matter of fact, the sample containing uncured EPR (A), for crystallization temperatures closer to T'_m, shows the same T'_m as the plain iPP, a lower T'_m value being exhibited when reducing crystallization temperature further. On the other hand, for a given T_c, a noticeable depression in T'_m values is shown by the blend sample containing cured EPR (B).

The crystallinity index of the iPP–EPR blends [X_c(blend)] and of the iPP phase [X_c(iPP)] are reported in Table III as a function of T_c. Note that both X_c(blend) and X_c(iPP) increase with increasing T_c. Moreover, for a given T_c, the X_c(blend) values are much lower than that of the plain iPP, and the lowest X_c(blend) value is shown by the blend sample containing cured EPR (B). It is interesting to note, moreover, that for a given T_c the X_c(iPP) values shown by the iPP phase crystallized in presence of EPR and cured EPR are lower than that shown by the plain iPP, the lowest crystallinity being shown by the blend sample with cured EPR. Such findings indicate that the presence of the EPR (70% wt/wt) rubbery phase noticeably influences the isothermal crystallization process of iPP, such an influence becoming stronger when the EPR phase is cured. It has also to be taken into account that, by means of the curing agent, branching may be undergone by the iPP phase during the dynamic vulcanization process. Therefore the iPP phase crystallized in presence of the cured EPR could have a different molecular structure.

Phase Structure

Microscopy Studies

Optical micrographs, taken with parallel polars, of thin films of the iPP–EPR blends, kept at about 40°C above the iPP apparent melting temperature (T'_m), are shown in Figure 2. As shown, both A and B samples exhibit phase separation in the melt indicating that the blend components are immiscible above the iPP T'_m.

Figure 3 shows optical micrographs, taken with crossed polars, of quenched thin films of the plain iPP and iPP–EPR blends. As expected, the plain iPP crystallizes in a microspherulitic superstructure [see Fig. 3(a)]. The iPP phase crystallized in presence of EPR [see Fig. 3(b)] and cured EPR [see Fig. 3(c)] also exhibits microspherulitic superstructure. Note that such microspherulites appear in size to be lower than those of the plain iPP; moreover there seems to be no visible effect of the curing of the EPR rubbery phase on the iPP microspherulitic texture [compare Fig. 3(a) with 3(c)].

SEM micrographs of cryogenically fractured surfaces of quenched thin films of the iPP–EPR blends are shown in Figures 4 and 5. Sample A clearly shows phase separation (see Fig. 4); the iPP phase, in fact, appears to be the minor component, segregating in its own domains randomly distributed into the EPR rubbery matrix. Such domains, moreover, are irregular in shape and very different in size, indicating

Table III Overall Blend Crystallinity, X_c (Blend), and Crystallinity of iPP Phase, X_c (iPP), for Plain iPP and iPP Crystallized Isothermally from Its Blends with EPR Copolymer (A) and Cured EPR Copolymer (B) as a Function of Crystallization Temperature, T_c

	T_c = 124°C		T_c = 134°C		T_c = 139°C	
Sample	X_c (Blend) %	X_c (iPP) %	X_c (Blend) %	X_c (iPP) %	X_c (Blend) %	X_c (iPP) %
iPP	—	42	—	44	—	47
A	11	35	11	36	13	42
B	8	27	10	34	10	36

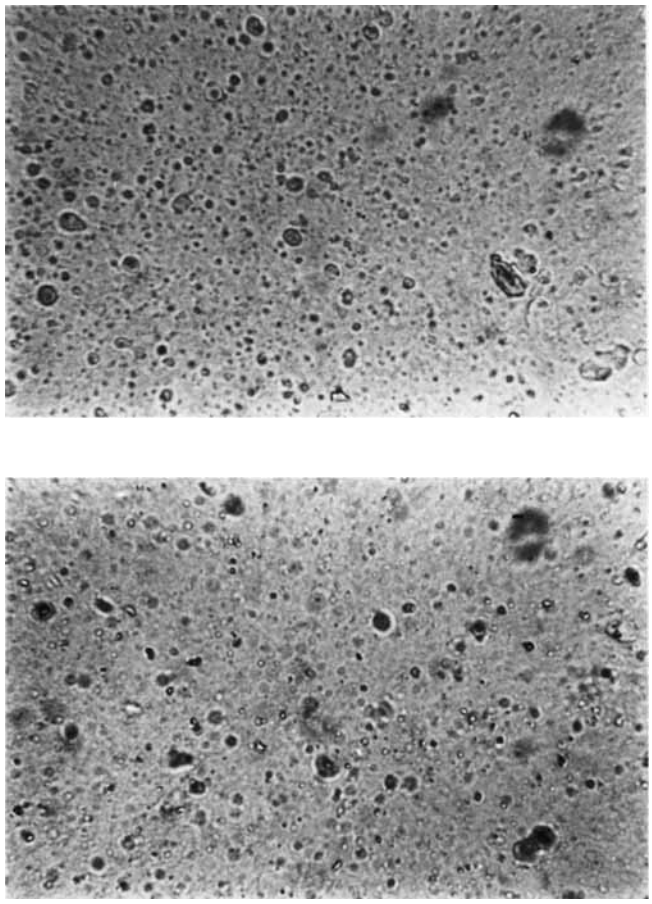

Figure 2 Optical micrographs, taken with parallel polars, of melted A (2a) and B (2b) blends.

that a low dispersion of the semicrystalline phase is achieved. A dramatic change in the morphology of the blends by curing the EPR component is observed (see Fig. 5). As shown, it cannot be determined which phase is continuous and which one dispersed. The fracture surface of sample B is characterized by the presence of domains, more or less spherical in shape, exhibiting an extremely short interparticellar distance. The size of such domains, presumably ascribed to cured EPR phase, ranges between 0.8 and 2.0 μm.

To better elucidate the phase structure developed in such a blend, cryogenically fractured surfaces of B-quenched sheets have been etched with boiling xylene vapors for 30 min. SEM micrographs of these etched surfaces are shown in Figure 6. As shown, and as expected, many vulcanized touching rubber particles are observed. The size distribution of such particles is found to be broader (0.25–2.25 μm) than that, in the first approximation, measured. It is very interesting to discover that the iPP phase crystallizes in a structure that resembles a cobweb tending to surround the EPR-cured particles; the voids inside the cobweb represent the areas where the EPR uncured phase resided before the xylene extraction [see Fig. 6(a)]. Such findings indicate that, owing to the dynamic curing process of the EPR component, the iPP phase tends to become continuous in the melt; i.e., a phase inversion occurs. It should be pointed out, moreover, that the iPP cobweb seems to be constituted by row structures of stacked lamellae [see Fig. 6(c)]. Similar superstructures of stacked lamellar aggregates are observed in the hard elastic polypropylene fibers, which exhibit highly recoverable deformation.[18–21]

The above morphological results have been confirmed by means of the TEM analysis performed on ultrathin sections of B sample stained with RuO_4 (see Fig. 7). The RuO_4 preferentially stains the amorphous phase making it dark, whereas the crystalline phase remains bright, therefore in Figure 7 the completely dark areas and the bright areas represent the EPR and iPP phase, respectively.

Optical micrographs, taken with crossed and par-

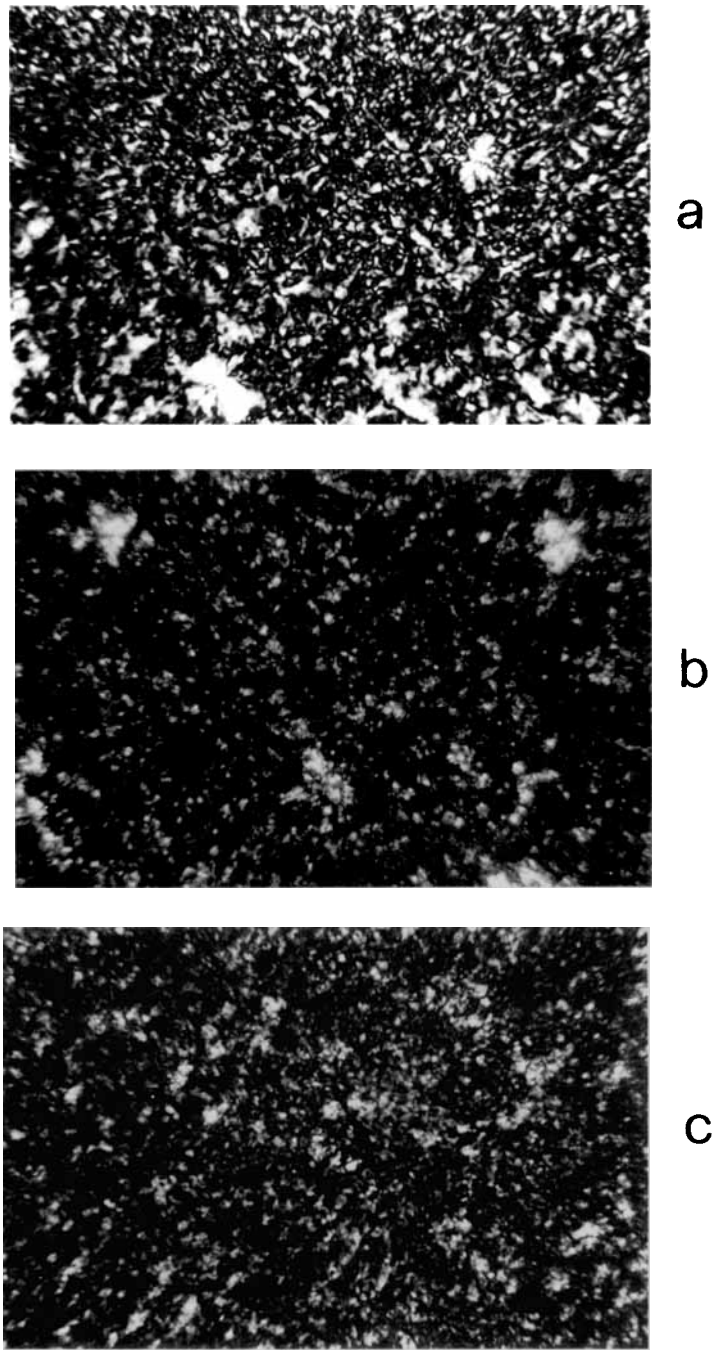

Figure 3 Optical micrographs, taken with crossed polars, of quenched sheet of plain iPP (3a) and of A (3b) and of B (3c) blends.

allel polars, of thin films of the plain iPP and iPP–EPR blends isothermally crystallized at 124, 134, and 139°C, are shown in Figures 8–10. As expected, the spherulite size of the plain iPP increases with increasing T_c. Moreover at relatively high T_c (139°C) large amorphous interspherulitic contact regions can be observed, in agreement with results already obtained while studying the isothermal crystallization process of a different sample of iPP.[15] This finding supports that, for the lowest T_c (T_c = 124°C), the amorphous material is predominantly located in the intraspherulitic regions, whereas with higher T_c it tends more and more to be rejected into interspherulitic contact regions. It is to be pointed

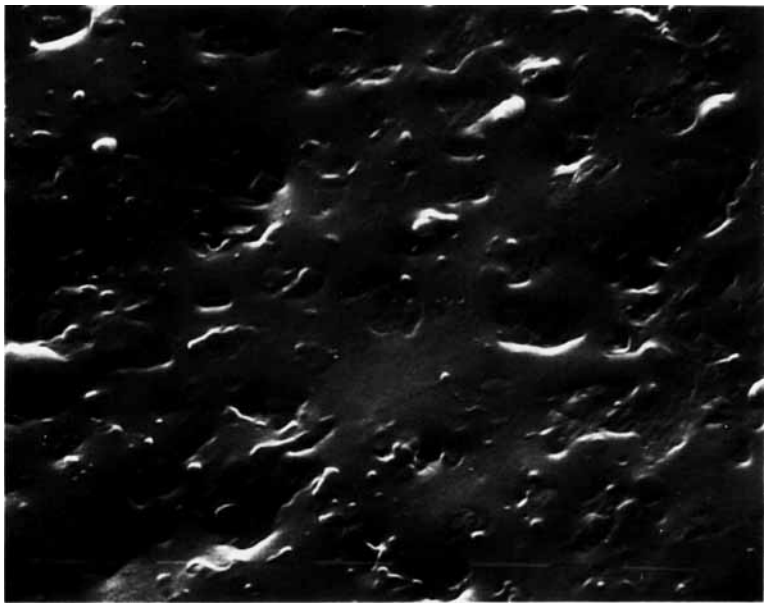

Figure 4 SEM micrograph of cryogenically fractured surface of quenched sheet of blend A (1250×).

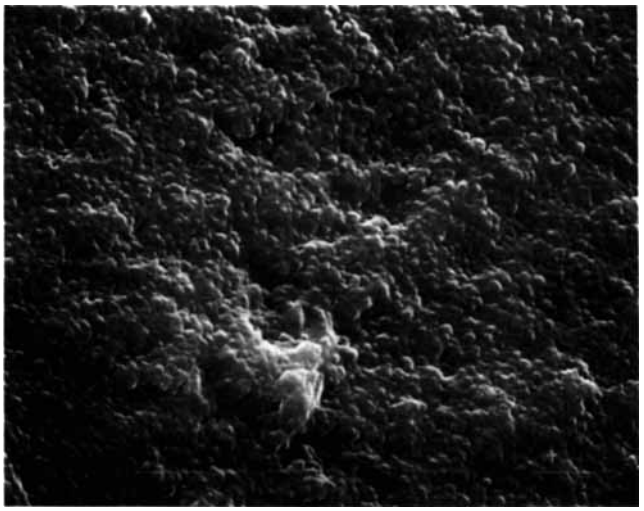

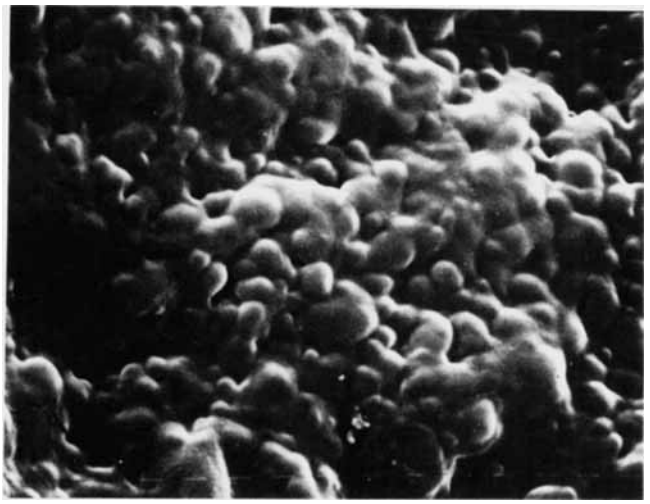

Figure 5 SEM micrographs of cryogenically fractured surfaces of quenched sheet of blend B: (a) 1250× and (b) 5000×.

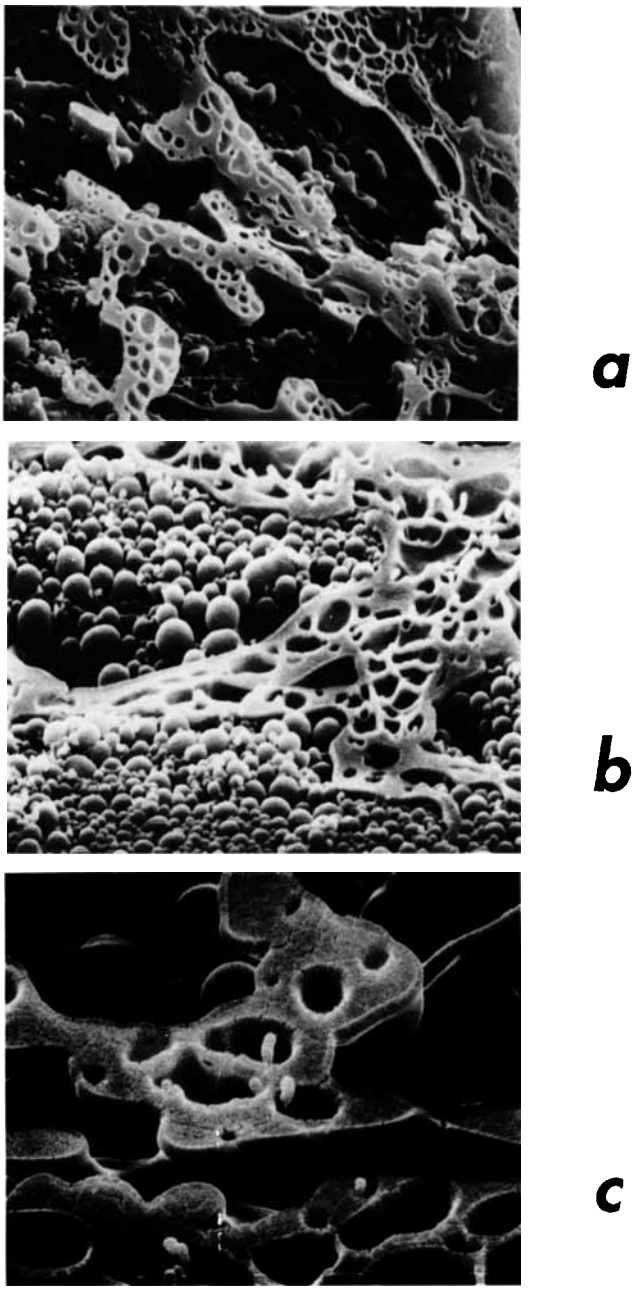

Figure 6 SEM micrographs of etched cryogenically fractured surface of quenched sheet of blend B: (a) 1250×, (b) 5000×, and (c) 10,000×.

out that when the iPP phase is allowed to isothermally crystallize in presence of 70% (wt/wt) of EPR and cured EPR, spherulites are formed whose size, neatness, and regularity are dramatically modified. For a given T_c the size, neatness, and regularity of the spherulites of iPP crystallized from its blends with both EPR and cured EPR strongly decrease, the extent of such a decrease increasing with T_c. Moreover, as shown in Figures 8–10, irrespective of T_c and copolymer molecular structure, the iPP phase remains microspherulitic in its superstructure; such a superstructure being comparable to that shown by the nonisothermally crystallized iPP phase in the quenched blend samples (compare Fig. 3 with Figs. 8–10).

Wide-Angle X-Ray Scattering Studies

Typical WAXS diffractograms of plain iPP and iPP–EPR blends isothermally crystallized are shown

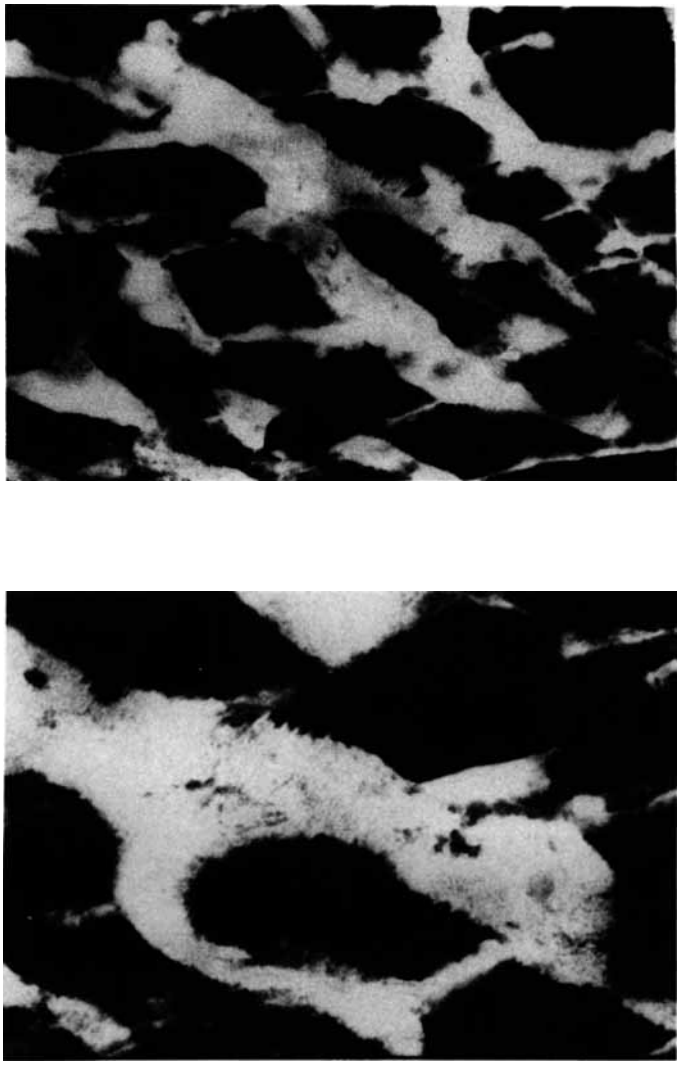

Figure 7 TEM micrographs of thin sections of etched surfaces of blend B: (a) 13,000× and (b) 20,000×.

in Fig. 11; it can be observed that, with increasing T_c, in agreement with DSC results, the intensity of the crystalline peaks increases.

The apparent crystal size (D) of iPP in the perpendicular direction to the (110) and (040) crystallographic planes was calculated by the Sherrer equation[14]:

$$D_{hkl} = \frac{K\lambda}{\beta_0 \cos(\theta_{hkl})} \quad (1)$$

where β_0 is the half width in radians of the reflection corrected for instrumental broadening; λ is the wavelength of the radation used (1.5418 Å). The shape factor K is set equal to unity and so the size data have to be considered as relative data.

The crystal size D of the plain iPP are consistently higher than for the blends. It is to be noted that the D decrease seems to be influenced by the EPR molecular structure, comparatively lower D being shown by iPP crystallized in the presence of cured EPR (see Table IV). Such findings could suggest a lower growth of the iPP crystals in the blends; moreover such a growth seems to be further lowered when the iPP phase crystallizes in the presence of the cured EPR.

Small-Angle X-Ray Scattering Studies

Typical Lorentz-corrected desmeared patterns for the plain iPP and iPP–EPR blends are shown in Figs. 12 and 13. As shown, the desmeared SAXS profiles of the plain iPP and iPP crystallized in presence of the EPR copolymer exhibit well-defined

Figure 8 Optical micrographs, taken with crossed polars, of thin films of the plain iPP isothermally crystallized at 124, 134, and 139°C.

maxima; on the contrary no maxima from the desmeared SAXS profiles of the iPP crystallized in the presence of cured EPR can be detected. By applying Bragg's law, the long period L, calculated from the peak position, was obtained for the plain iPP and iPP–EPR blend as a function of T_c. Assuming a two-phase model for the iPP spherulite fibrillae, consisting of alternating parallel crystalline lamellae and amorphous layers, from the L values the crystalline lamellar thickness, L_c was calculated using the following relation:

$$L_c = \frac{X_c L}{(\rho_c/\rho_a)(1 - X_c) + X_c} \tag{2}$$

where X_c is the DSC crystallinity index of the iPP

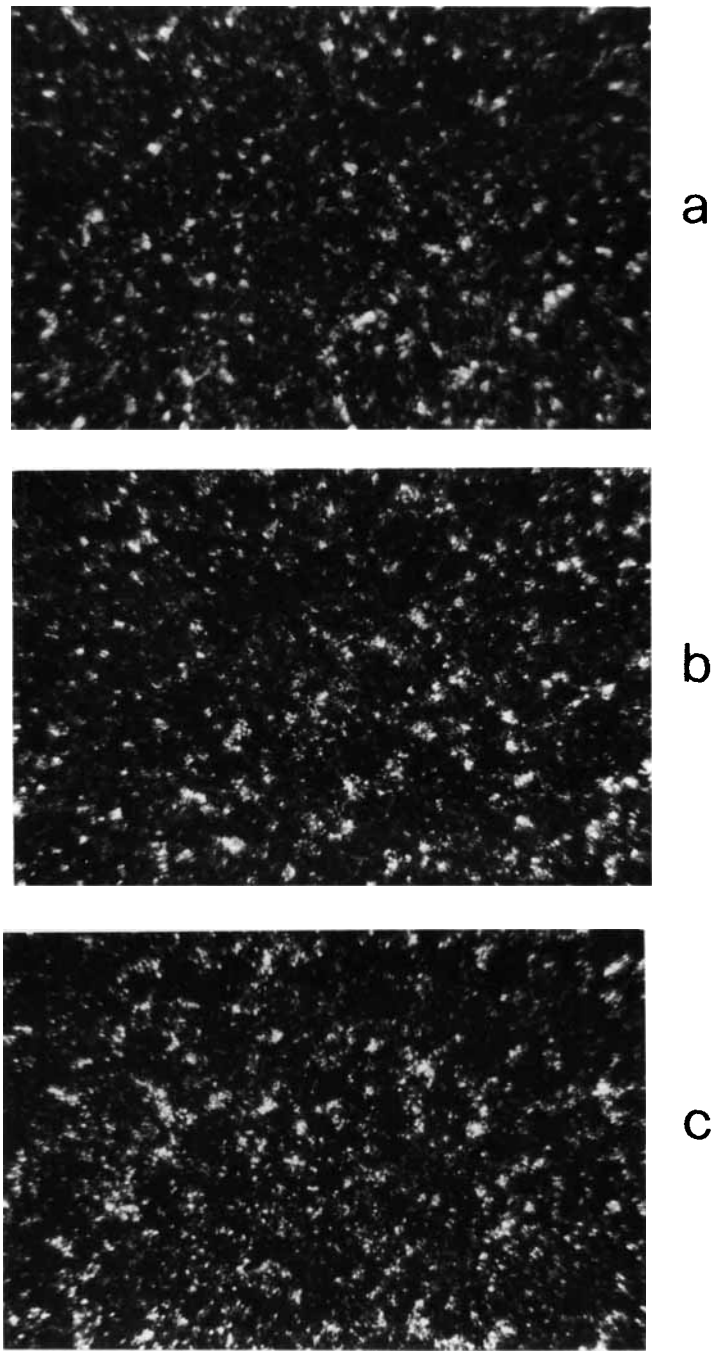

Figure 9 Optical micrographs, taken with crossed polars, of thin films of A blend at 124, 134, and 139°C.

phase, ρ_c and ρ_a are the densities of the crystalline and amorphous iPP phase, respectively. Subtracting the values of L_c obtained from the L values the average thickness of the amorphous interlamellar layers, L_a, was obtained. The L values for the plain iPP ($L_{(iPP)}$) and iPP–EPR blend ($L_{(iPP\text{-}EPR)}$) are reported in Table V as a function of T_c. As expected, both $L_{(iPP)}$ and $L_{(iPP\text{-}EPR)}$) increase with increasing T_c. To reiterate, no L values can be detected for the iPP crystallized in presence of cured EPR. This result suggests that the iPP phase crystallized in presence of cured EPR could be characterized by L values significantly larger than those of plain iPP and iPP–EPR blends or by a wide distribution of the long period. Finally, the L values shown by the plain iPP and iPP crystallized from its blends with EPR co-

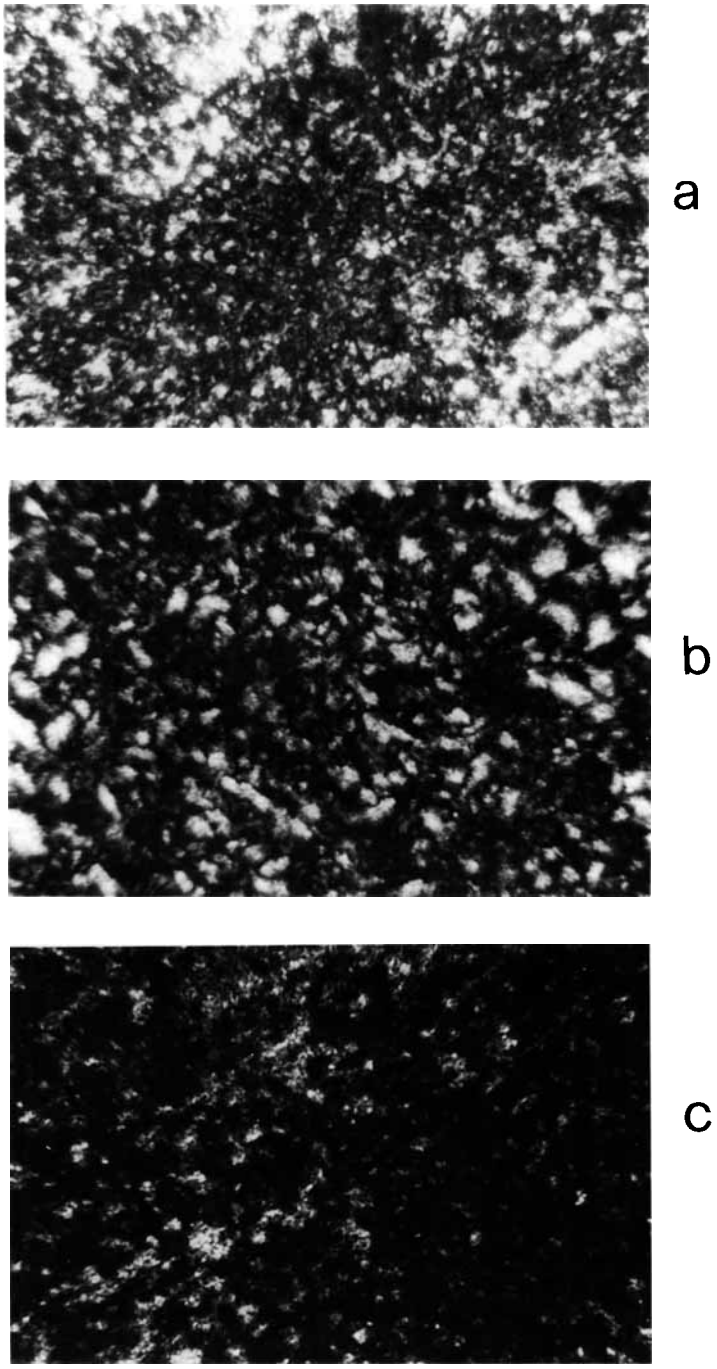

Figure 10 Optical micrographs, taken with crossed polars, of thin films of B blend at 124, 134, and 139°C.

polymer are to be considered the same within experimental error (+5 Å) with no dependence on EPR content (wt/wt).

The L_c and L_a values for the plain iPP ($L_{c(\text{iPP})}$ and $L_{a(\text{iPP})}$) and iPP–EPR blends ($L_{c(\text{iPP-EPR})}$ and $L_{a(\text{iPP-EPR})}$) are reported in Table VI as a function of T_c. As shown, as expected, the $L_{c(\text{iPP})}$ and $L_{c(\text{iPP-EPR})}$ values increase with increasing T_c. For a given T_c, it is notable that $L_{c(\text{iPP-EPR})}$ and $L_{a(\text{iPP-EPR})}$ are, respectively, lower and higher than that of the plain iPP. Thus, when iPP crystallizes from its blends in the presence of EPR (70% wt/wt) phase, lamellar crystals are formed whose thickness, measured along a direction that is almost

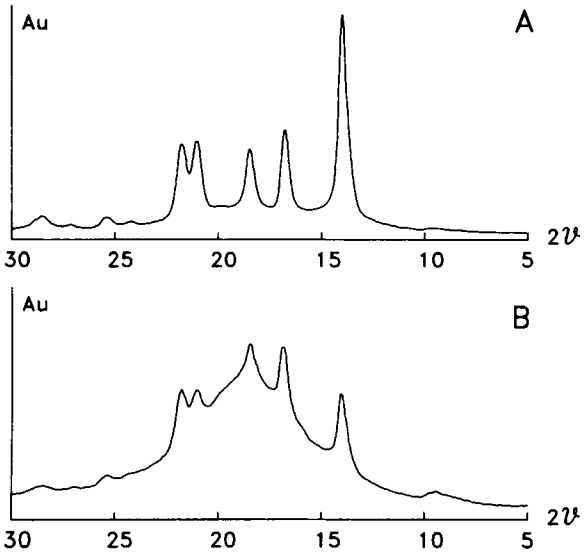

Figure 11 WAXS patterns of (a) iPP and (b) blend A isothermally crystallized at 124°C.

coincident with the chain axis, is lower than that of the plain iPP. Moreover, the phase structure is characterized by interlamellar amorphous layers with increased thickness.

Table IV Apparent Crystal Size *D* of the Plain iPP and Blends in Perpendicular Direction to the (110) and (040) Crystallographic Planes

	Apparent Crystal Size (D) of Plain iPP and Blends (Å)					
	T_c = 124°C		T_c = 134°C		T_c = 139°C	
Sample	(110)	(040)	(100)	(040)	(100)	(040)
iPP	198	210	254	199	296	198
A	187	198	198	188	198	188
B	162	179	187	198	170	178

Plotting the apparent melting temperature (T'_m) obtained by DSC of the plain iPP and iPP crystallized in the presence of EPR versus the inverse of lamellar thickness ($1/L_c$) straight lines can be drawn. Therefore, the trend of T'_m against $1/L_c$ can be described by the following relation[22]:

$$T'_m = T_m - \frac{2\sigma_e T_m}{\Delta H_f^\circ} \frac{1}{L_c} \qquad (3)$$

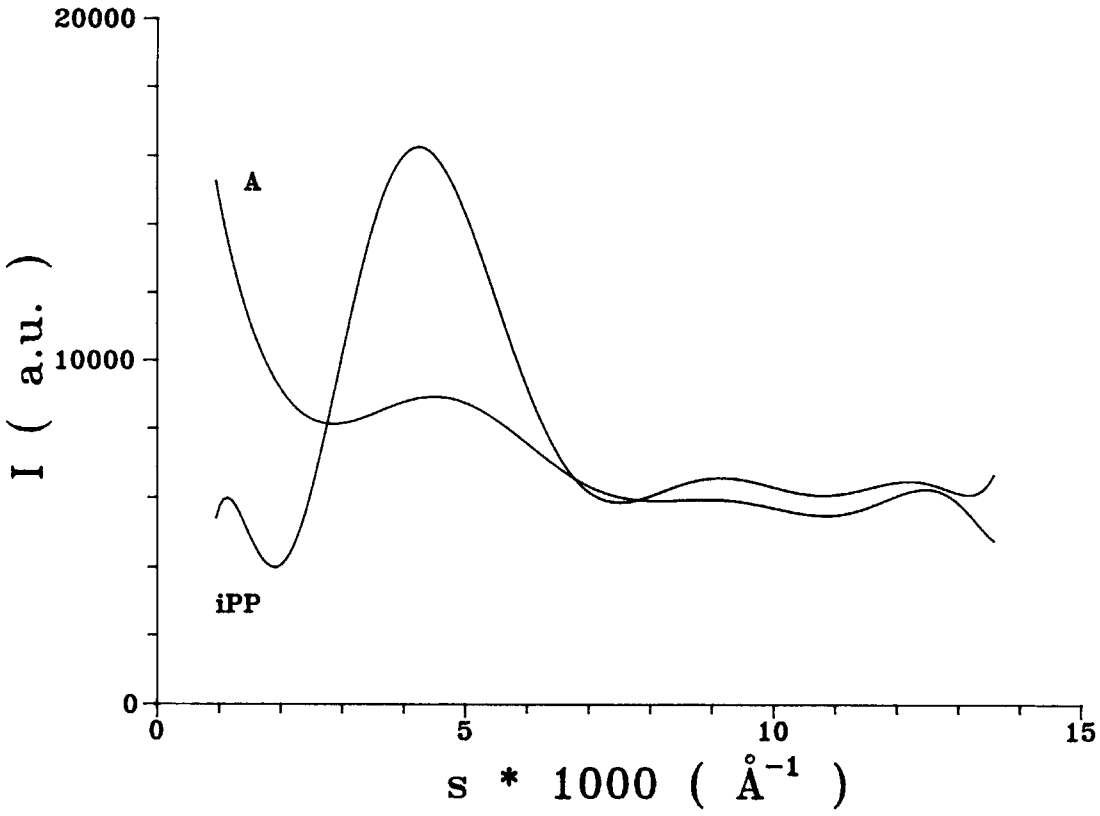

Figure 12 Comparison between the desmeared SAXS patterns of plain iPP and its blend with uncured EPR.

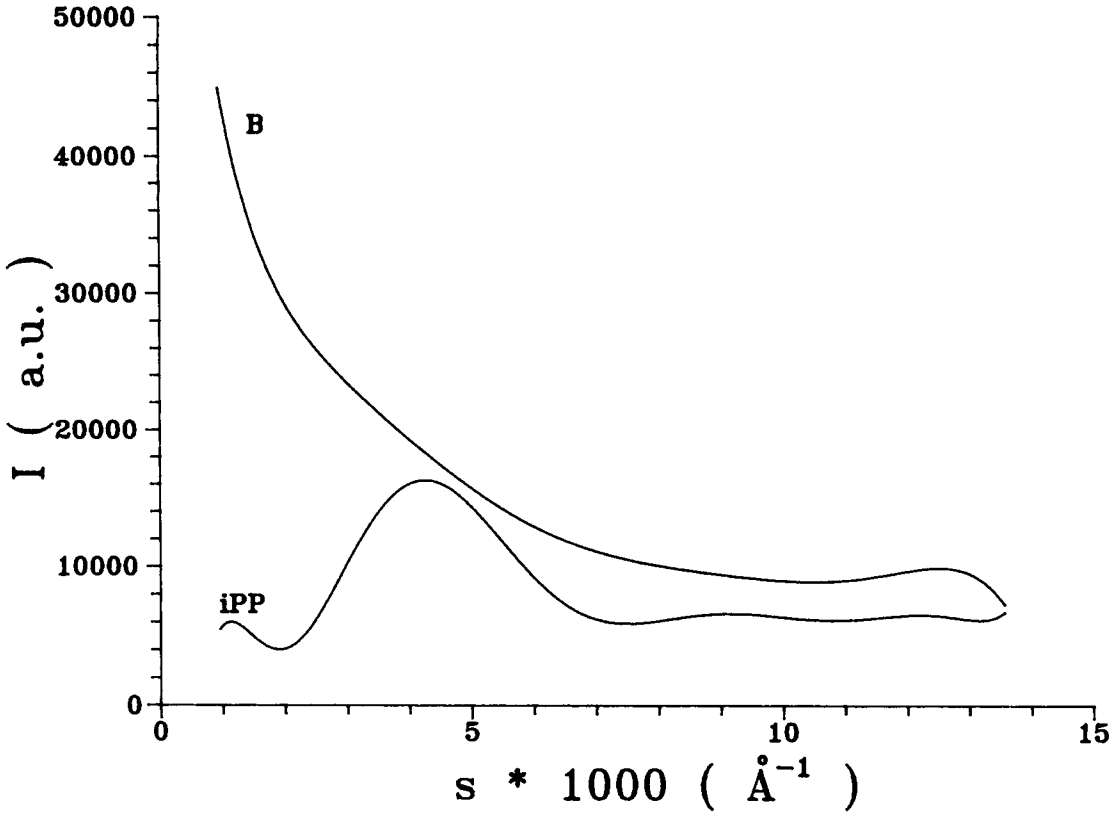

Figure 13 Comparison between the desmeared SAXS patterns of plain iPP and its blends with cured EPR.

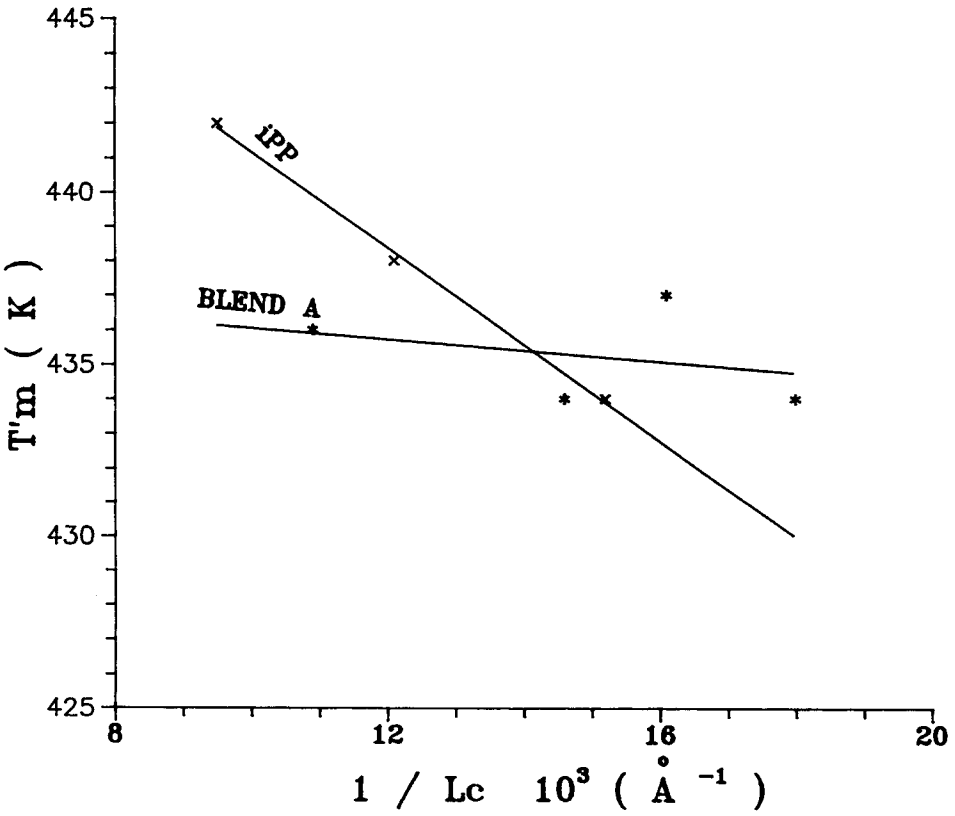

Figure 14 Plot of the observed melting temperature (T'_m) as a function of the reciprocal of the lamella crystal thickness ($1/L_c$): (×) iPP, (*) blend A.

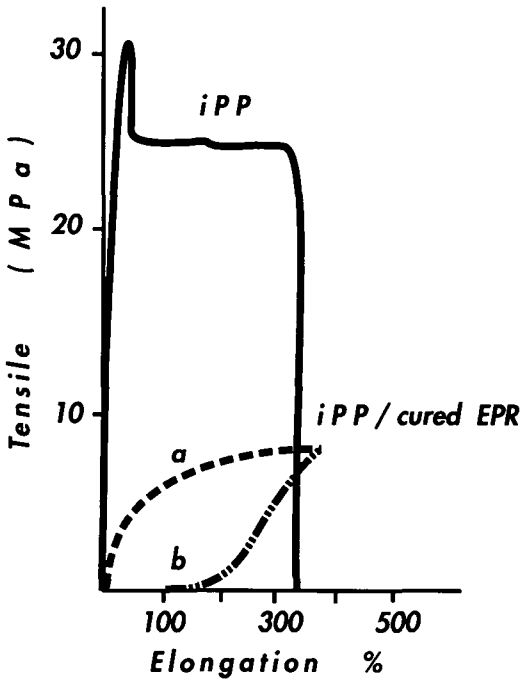

Figure 15 Typical extension and retraction curves for plain iPP and B sample.

where T'_m is the apparent melting temperature, T_m the equilibrium melting temperature, σ_e the free energy of folding, ΔH_f° the enthalpy of fusion of 100% crystalline iPP,[12] and L_c the lamellar crystal thickness. According to Eq. (3) T_m and σ_e can be determined, respectively, from the intercept and slope of the straight lines obtained by plotting T'_m against $1/L_c$. As shown in Figure 14 for the plain iPP this equation fits the experimental data quite well, a comparatively worse fit being obtained for the iPP–EPR blends. The T_m and σ_e values determined by this method for the plain iPP are, respectively, 455 K and 77 erg/cm^2, in agreement with the values reported in literature.[12]

The T_m value obtained for iPP crystallized in the presence of EPR is about 16 K lower than that of the plain iPP (439 K). Such a finding is in agreement with results obtained in previous work showing that the T_m (iPP–EPR) values tend to be depressed with increasing EPR content in the blend. Taking into account that iPP and EPR are immiscible in the melt, such a lowering could be ascribed to kinetic and morphological effects rather than to a thermodynamic effect.

A very strong depression in $\sigma_{e(\text{iPP/EPR})}$ value is also observed. This depression indicates that the iPP crystals, grown in the presence of an EPR phase, have much less regular surface and supports results obtained in previous work;[15] when iPP crystallizes from its blends with EPR copolymers, crystals are formed whose surface becomes more irregular the higher the EPR content is in the blend.

MECHANICAL BEHAVIOR

Typical stress–strain curves for sample B are reported in Figure 15. As shown, by comparing part (a) of the curve relative to the increasing deformation with part (b) of the curve relative to the decreasing deformation, sample B exhibits classical elastomeric behavior. The deformation recovery is practically complete even for large values of the strain. Elastomeric behavior is shown by the B material, in spite of the presence of the crystalline iPP connecting matrix. The neat iPP, in fact, as is well known, shows very low recovery for an imposed large deformation (see Fig. 15).

The mechanical behavior shown by B sample could be accounted for by considering the particular phase structure generated in the material. Such phase structure could be modeled according to Fig. 16. As shown, the cured EPR particles and the iPP matrix are, respectively, represented, in schematic form, by the shadowed circles and the white area; the row structures of stacked lamellae of the iPP, SEM, and TEM observed, are represented by springs. Such row structures, moreover, seem to be quite comparable to those observed in the "hard elastic polypropylene",[18-21] which also exhibits very large deformation recovery. The model accepted for explaining the elastic behavior of such polypropylene is the so-called leaf-spring model. In such a model, the individual lamellae in the stacks are each joined to their top and bottom neighbors by a network of tie points with unconnected areas between lamellae. Owing to this particular geometry, the stacked lamellae polypropylene can undergo almost complete elastic recovery even for large deformation.

It could be reasonably hypothesized, on the basis

Table V Long Spacing (L) for Plain iPP and iPP Crystallized Isothermally from Its Blends with EPR Copolymer (A) and Cured EPR Copolymer (B) as a Function of Crystallization Temperature, T_c

	L (Å)		
Sample	T_c = 124°C	T_c = 134°C	T_c = 139°C
iPP	167	197	235
A	169	184	231
B	/	/	/

Table VI Crystalline Lamella Thickness, L_c, and Interlamellar Amorphous Layer Thickness, L_a, for Plain iPP and iPP Crystallized Isothermally from Its Blends with EPR Copolymer A as a Function of Crystallization Temperature, T_c

	T_c = 124°C		T_c = 134°C		T_c = 139°C	
Sample	L_c (Å)	L_a (Å)	L_c (Å)	L_a (Å)	L_c (Å)	L_a (Å)
iPP	66	101	83	114	106	129
A	56	114	62	122	92	139

of the morphological results, that the leaf-spring model applies also to the iPP phase in the thermoplastic elastomers investigated.[23] According to this hypothesis, the row structures of stacked lamellae shown by the iPP phase allow the material to behave elastically. Finally such a phase structure model could account for the desmeared SAXS patterns exhibited by iPP crystallized in the presence of cured EPR.

CONCLUDING REMARKS

A study, aimed at establishing the phase morphology and structure developed in samples of (30/70) iPP–EPR and iPP–cured EPR blends, nonisothermally crystallized and isothermally crystallized at temperature relatively close to T'_m, has been performed.

The following results are noted:

1. The process of dynamic curing of the EPR component dramatically affects the phase morphology and structure development in the material. The blend containing the uncured EPR component is characterized by the presence of iPP domains randomly distributed in the EPR rubbery matrix, whereas in the blend containing the cured EPR component the iPP phase is the continuous phase. The iPP phase, in fact, crystallizes in a structure that resembles a cobweb surrounding the EPR-cured particles. Moreover the iPP phase crystallizes under stress in row structures of stacked lamellae similar to that observed in the hard elastic polypropylene.
2. The melting behavior of the iPP phase in iPP–EPR blends is confirmed to be independent of the overall blend composition and EPR molecular mass according to results obtained in previous work.[15] On the contrary, the thermal behavior of the iPP phase crystallized in the presence of cured EPR is strongly affected by the presence of cured rubbery component, a noticeable depression in T'_m value being found.
3. The isothermal crystallization process of the iPP from its blends with EPR and cured EPR is noticeably influenced by presence of the rubbery phase, a comparatively stronger influence being observed for samples containing cured EPR. For a given T_c, the crystallinity index of the iPP phase, crystallized in the presence of the EPR and the cured EPR phase, is lower than that shown by the plain iPP; the lowest crystallinity being shown by the iPP phase crystallized in the presence of the cured EPR phase. Optical investigation revealed, moreover, that the iPP phase, irrespective of both T_c and molecular structure of the EPR copolymer, remains microspherulitic in its superstructure, such a superstructure being comparable to that shown by the iPP phase in the quenched blend samples.
4. The desmeared SAXS profiles shown by the iPP phase, crystallized in presence of the uncured EPR phase, show well-defined maxima.

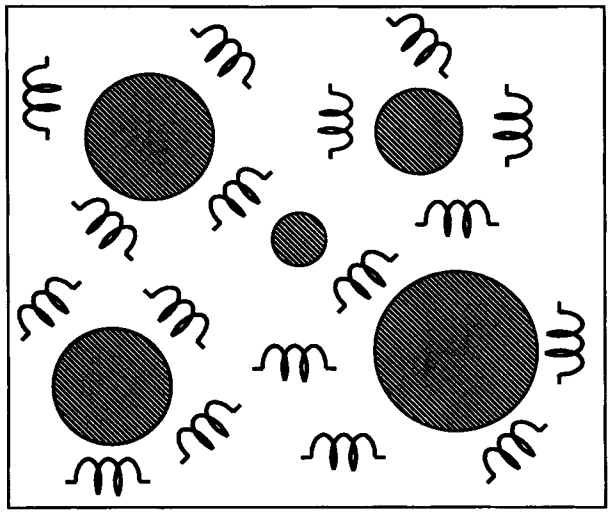

Figure 16 Schematic model of the phase structure generated in B material.

On the contrary, no maxima, irrespective of T_c, from the desmeared SAXS profiles of the iPP phase crystallized in presence of cured EPR phase can be detected. Furthermore, for a given T_c, the thickness of the crystalline lamella of the iPP crystallized in presence of the uncured EPR decreases, whereas the thickness of the amorphous interlamellar layer increases.

5. Other thermodynamic parameters of the iPP lamellar crystal growth in the presence of the uncured EPR phase are found to be strongly influenced by the presence of the rubbery component. In fact both the equilibrium melting temperature (T_m) and the surface free energy of folding (σ_e) of the iPP crystals are highly depressed.
6. The elastic behavior of the vulcanized thermoplastic elastomer has been accounted for by applying the leaf-spring model to the morphology and structure of the iPP phase.

This work was partially supported by Progetto Finalizzato "Chimica Fine II" of C.N.R.

REFERENCES

1. E. N. Kresge, in *Polymer Blends,* D. R. Paul and S. Newman, Eds., Academic Press, New York, 1978.
2. N. R. Legge, G. Holden, and H. E. Schreoder, *Thermoplastic Elastomers,* Hanser Publishers, New York, 1987.
3. A. M. Gessler, U.S. Pat. 3,037,954 (June 5, 1962).
4. *Rubber World,* February, 1973, p. 49.
5. W. K. Fisher, U.S. Pat. 3,758,643 (Sept. 11, 1973).
6. W. K. Fisher, U.S. Pat. 3,806,558 (April 23, 1974).
7. *Rubber World,* October, 1970, p. 59.
8. P. F. Hartman, U.S. Pat. 3,909,463 (Sept. 30, 1975).
9. A. Y. Coran, B. Das, and R. P. Patel, U.S. Pat. 4,130,535 (Dec. 19, 1978).
10. A. Y. Coran and K. Patel, *Rubber Chem. Technol.,* **53,** 141, 1980.
11. V. Braga, M. Manica, E. Martini, and F. Milani, U.S. Pat. 4,963,612 (Oct. 1990).
12. S. Brandup and E. M. Immergut, *Polymer Handbook,* Interscience, New York, 1975, Vol. 5, p. 24.
13. C. G. Vonk, *J. Appl. Cryst.,* **8,** 340 (1975).
14. L. E. Alexander, *X-ray Diffraction Method in Polymer Science,* Wiley-Interscience, New York, 1969.
15. L. D'Orazio, C. Mancarella, E. Martuscelli, and G. Sticotti, *J. Mat. Sci.,* **26,** 4033 (1991).
16. E. Martuscelli, *Polym. Eng. Sci.,* **24**(8), 563 (1984).
17. E. Martuscelli, *Polym. Eng. Sci.,* **24**(15), 1155 (1984). (1984).
18. R. G. Quinn and H. Broyd, *J. Macromol. Sci.-Phys.,* **B5**(4), 721 (1971).
19. B. Cayrol and J. Petermann, *J. Polym. Sci. Polym. Phys. Ed.,* **12,** 2169 (1974).
20. B. S. Sprague, *J. Macromol. Sci. Phys.,* **B8**(1–2), 157 (1973).
21. E. N. Kresge, *J. Appl. Pol. Sci.-Appl. Polym. Symp.,* **39,** 37 (1984).
22. J. D. Hoffman, *Polymer,* **24,** 3 (1982).
23. V. Braga, R. Ghisellini, and E. Martini, Scandinavian Rubber Conference-Artic Rubber 89, Tampere (Finland), Proceedings B (1989).

Received April 5, 1993
Accepted May 18, 1993